



# Graphene oxide-based zirconium oxide nanocomposite for enhanced visible light-driven photocatalytic activity

Ranjita S. Das<sup>1</sup> · Swapnil K. Warkhade<sup>1</sup> · Anupama Kumar<sup>1</sup> · Atul V. Wankhade<sup>1</sup>

Received: 30 July 2018 / Accepted: 5 December 2018 / Published online: 1 January 2019  
© Springer Nature B.V. 2019

## Abstract

In the present investigation, an efficient visible light-active, graphene oxide-based zirconium oxide nanocomposite (GO–ZrO<sub>2</sub>) has been synthesized by co-precipitation method. The synthesized photocatalyst was characterized by XRD, FTIR, FE-SEM, EDS, TEM, TGA, PL, UV-DRS and BET surface area analysis. The characterization results illustrate the homogeneous dispersion of ZrO<sub>2</sub> nanoparticles in the GO–ZrO<sub>2</sub> nanocomposite with excellent harmony between GO and ZrO<sub>2</sub> nanoparticles. The photocatalytic efficiency of the synthesized GO–ZrO<sub>2</sub> nanocomposite was evaluated by photodegradation of hazardous, water-soluble rhodamine B and methylene blue dyes under visible light irradiation. The 90% photocatalytic degradation of rhodamine B dye (with initial conc. 30 mg/L) was observed in 105 min of visible light irradiation, while 99.23% of methylene blue (with initial conc. 100 mg/L) dyes degradation was observed in just 60 min using 25 mg/100 ml dose of GO–ZrO<sub>2</sub> nanocomposite as a photocatalyst. The mechanistic investigation using scavengers suggest that the superoxide (O<sub>2</sub><sup>•-</sup>) is the most reactive species involved in the photodegradation of organic dyes. The synthesized photocatalyst GO–ZrO<sub>2</sub> nanocomposite also exhibits excellent thermal stability and reusability.

**Keywords** Graphene oxide · Zirconium oxide · Co-precipitation method · Rhodamine B · Methylene blue · Visible light · Photocatalytic activity

**Electronic supplementary material** The online version of this article (<https://doi.org/10.1007/s11164-018-3699-z>) contains supplementary material, which is available to authorized users.

✉ Atul V. Wankhade  
atulwa2006@yahoo.co.in

<sup>1</sup> Department of Chemistry, Visvesvaraya National Institute of Technology, Nagpur 440010, India

## Introduction

According to the WHO (World Health Organization) in 2015, 663 million people are affected by the shortage of drinking water because of water pollution [1, 2]. In this context, the heterogeneous photocatalytic oxidation of organic pollutants in aqueous media has brought about advances in scientific research [2, 3]. Various investigations have proven that synthetic dyes possess carcinogenic, mutagenic and allergenic properties. In spite of this, these dyes have been extensively used in many industries such as paper, textiles, cosmetics, pharmaceuticals, and printing as a colorant due to their easy availability [4, 5]. Discharge of these organic pollutants into the ecosystem can cause serious environmental and human health concerns [6, 7]. The conventional treatment is not a suitable remedy for these environmental issues; therefore, attention has been shifted to photocatalysis as a promising option to mineralize organic pollutants into  $\text{CO}_2$ ,  $\text{H}_2\text{O}$  and mineral acid [8–10]. Photocatalytic degradation is an advanced oxidation process (AOP), which illustrates an excellent pathway to overcome the related concern arising from wastewater treatment, as it is easy to operate, takes less time, has a fast occurring reaction and low-cost production [11]. Various semiconductor photocatalysts such as  $\text{TiO}_2$ ,  $\text{ZnO}$ ,  $\text{ZnS}$  nanoparticles,  $\text{MgO}$ ,  $\text{ZrO}_2$ ,  $\text{CeO}_2$ ,  $\text{SnO}_2$ ,  $\text{WO}_3$ , and  $\text{Fe}_2\text{O}_3$  have been reported for the degradation of organic pollutants [12–14]. Among them, zirconium oxide ( $\text{ZrO}_2$ ) is a photocatalyst with both properties of oxidizability and reducibility because of its acidic and basic nature [15].  $\text{ZrO}_2$  based composites exhibit various applications in different fields such as removal of chlorophenol [16], phosphate ions [17], fluoride and lead ions [18], biosensing, electrochemical sensing [19] and photocatalytic degradation of organic pollutants [20].  $\text{ZrO}_2$  is widely used as a heterogeneous photocatalyst because it has excellent properties such as inert chemical and physical nature, low toxicity, chemical and photothermal stability, high corrosion resistance, low thermal conductivity and less production cost [8]. But,  $\text{ZrO}_2$  also possesses some limitations, such as low quantum efficiency due to high recombination rate of the photogenerated electron–hole pairs and wide bandgap [1, 3]. To improve the photocatalytic efficiency of  $\text{ZrO}_2$ , mostly doping of transition metals and non-metals [8, 26, 31] and loading with carbon-based materials such as graphitic carbon nitride [21, 22], carbon nanotubes [23], graphene (GR) [24] and reduced graphene oxide (rGO) [15] has been reported.

Recently, graphene has become a promising material because of its good electrical conductivity, high transparency and the large specific surface area, which makes it an excellent material for the adsorption of many pollutants [25]. However, GO is a derivative of graphene with a large number of oxygen-containing functional groups and exhibits excellent properties such as larger surface area, high mechanical, thermal and optical properties, which makes it outstanding base material compared to other carbon derivatives [26]. The literature suggests that  $\text{ZrO}_2$  has a strong affinity towards negatively charged moiety, thus incorporation of carbon-based materials with metal oxide improves the catalytic activity of the catalyst [16]. Moreover, a few works have also reported on  $\text{ZrO}_2$  based

composites such as  $\text{ZrO}_2/\text{ZnO}$  nanocomposite (degrades Rh-B 9 ppm in 180 min) [1], doping of Gd, C, N, S- $\text{ZrO}_2$  (degrades indigo carmine 20 ppm in 210 min) [3], doping of Eu, C, N, S- $\text{ZrO}_2$  (degrades indigo carmine 20 ppm in 210 min) [8], composite of  $\text{MgO-ZrO}_2$  (decomposes basic blue 9 dye 5 ppm in 60 min) [12], composite of  $\text{Fe}_3\text{O}_4\text{-ZrO}_2$  (decomposes methyl orange 10 ppm in 235 min) [27] and composite of Cr-doped  $\text{SO}_4^{2-}/\text{ZrO}_2$  (photodegradation of methylene blue of 10 ppm dye solution in 120 min) [28]. A few research papers have reported on a composite of  $\text{ZrO}_2$  with graphene [29] and graphene derivatives; however, these reported composites suffer from low-efficiency photocatalysis. There are few reports on GO- $\text{ZrO}_2$  nanocomposite with other application such as electrochemical sensors and supercapacitors [30]. Neodymium doped  $\text{ZrO}_2$ -graphene oxide (Nd- $\text{ZrO}_2$ -GO) nanocomposite reports the degradation of only 20 ppm eosin Y dye [31], and some papers report on the removal of inorganic metals such as As(III), As(V) and Cr(VI) ion [32, 33], but only  $\text{ZrO}_2$  on GO nanosheets has not yet been reported for the photocatalytic degradation of organic pollutants.

Inspired by these observations, we have fabricated a GO- $\text{ZrO}_2$  nanocomposite (NC) by facile co-precipitation method. This synthesized GO- $\text{ZrO}_2$  NC was employed for the photocatalytic degradation of Rh-B and MB dye solution with higher concentration. Furthermore, percent degradation, degradation kinetics, reusability and mechanism have been investigated in detail.

## Experimental section

Graphite powder (Sigma-Aldrich 99.99% purity), 98% sulfuric acid ( $\text{H}_2\text{SO}_4$ ), potassium permanganate ( $\text{KMnO}_4$ ), 30% hydrogen peroxide ( $\text{H}_2\text{O}_2$ ), hydrochloric acid (HCl), potassium hydroxide (KOH), zirconyl chloride octahydrate ( $\text{ZrOCl}_2 \cdot 8\text{H}_2\text{O}$ , 99.9% Merck), and ethanol (absolute 95% pure). All the chemicals used for synthesis are of analytical grade.

## Synthesis of photocatalyst

The fabrication of GO- $\text{ZrO}_2$  NC was carried out by facile co-precipitation method, and zirconium oxychloride salt ( $\text{ZrOCl}_2 \cdot 8\text{H}_2\text{O}$ ) was used as a precursor. In typical experiments, first of all, GO was synthesized by modified Hummers method applying graphite powder [34]. In detail, 0.5 g of GO was dispersed in 100 mL water by ultrasonication up to 30 min to separate out a single sheet of GO. To synthesize in situ GO- $\text{ZrO}_2$  NC, subsequently, 1 mmol of zirconium oxychloride was added and sonicated for another 30 min, followed by dropwise addition of 100 mmol potassium hydroxide solution in prepared suspension while maintaining the pH above 10.5 under stirring. The resulting precipitate was washed with distilled water for the removal of chloride ions, followed by washing with ethanol. Finally, the obtained product was allowed to dry in a vacuum oven at 60 °C overnight and calcined at 180 °C for 4 h in an airtight muffle furnace.

## Instrumentation

The crystalline structure of GO-ZrO<sub>2</sub> NC was studied by using X-Ray diffraction (XRD) [Model—AXS D8 Advance Bruker, Germany] with Cu-K<sub>α</sub> radiation ( $\lambda = 1.54056 \text{ \AA}$ ). The morphological and elemental mapping study were examined by scanning electron microscopy (SEM) [Model—JEOL 6380A] with EDS (energy dispersive X-ray spectroscopy) with a Joel apparatus [Model—JSM 5400]. Particle size distribution and d-spacing were measured by transmission electron microscopy (TEM) [Model—Joel/JEM 2100]. UV–Vis diffuse reflectance spectra (DRS) were studied by using a UV–Vis spectrophotometer instrument [Cary 5000]. The structural morphology of prepared materials was studied by conducting N<sub>2</sub> adsorption experiments on a Micromeritics ASAP 2020 V3.04H instrument at  $-196 \text{ }^\circ\text{C}$ . PL emission spectra of the samples were recorded at room temperature using a JASCO Spectrofluorometer (FP-8200). Effect of calcination on the percent weight loss was analyzed by using thermogravimetric analysis (TG) [TG-DTA-7200 Hitachi]. The Fourier transform infrared spectra (FTIR) were recorded for functional group determination by using a FTIR spectrometer [IR-Affinity-1, Shimadzu]. The diffuse reflectance spectra (DRS) of the photocatalyst were recorded by the UV–visible spectrophotometer [Shimadzu, Japan UV 1800].

## Photocatalytic activity evaluation

The photocatalytic activity of the as-prepared samples was evaluated by monitoring the degradation of methylene blue (MB) and rhodamine B (Rh-B) dye solution as our model organic pollutants. The experiment was carried out under visible light using a 100 W tungsten lamp (40 W/230 V Philips) as the simulated sunlight source in a locally made rectangular photoreactor. In each experiment, an optimized dose of 25 mg photocatalyst was dispersed into 100 mL of Rh-B (30 mg/L) and MB (100 mg/L) dye solution. Prior to illumination, the suspension was magnetically stirred in dark condition for 30 min to establish an adsorption–desorption equilibrium between the photocatalyst and dye solution. During irradiation, 5 mL of the suspension was sampled at an interval of 15 min and centrifuged to eliminate the catalyst particles. Finally, the supernatant was recorded to measure the concentration of dye solution using UV–vis spectrophotometer (UV-1800, Shimadzu) and the photocatalytic degradation efficiency was calculated from the following Eq. (1).

$$\text{Degradation} = \frac{C_o - C_t}{C_o} \times 100 \quad (1)$$

where  $C_o$  is the initial concentration of dye solution and  $C_t$  is the dye concentration at reaction time  $t$ .

## Results and discussion

The structural morphology of synthesized GO–ZrO<sub>2</sub> NC was studied by X-ray diffraction and was also compared with the diffraction pattern of GO and ZrO<sub>2</sub> as portrayed in Fig. 1. A poor and weak diffraction pattern was observed in the case of the synthesized GO–ZrO<sub>2</sub> NCs revealing the amorphous nature of the synthesized NC. The peaks in the diffraction pattern observed at  $2\theta$  31.23° and 51.32° corresponded to the (111) and (221) plane of monoclinic ZrO<sub>2</sub> nanoparticles while the sharp characteristic diffraction peak of GO was observed at  $2\theta$  11.43° and 42.00°, which corresponds to the (001) and (100) planes of GO, respectively. These diffraction peaks were significantly resembled with the standard JCPDS file (88-2390) of monoclinic ZrO<sub>2</sub> [20, 21] and previously reported diffraction peak for GO without any phase impurity [6, 15, 26]. In order to check the purity of the synthesized GO, the comparative diffraction pattern of pure graphite also has been given in Fig. 1a. The results revealed that the synthesized GO nanosheets do not have any phase impurity of pure graphite. From the detailed XRD analysis, GO has a higher inter-planer distance of 7.9 Å than the graphite at 3.31 Å. This shifting in inter-planer distance strongly supports that there were large numbers of oxygen-containing functional groups present on GO, which shows the complete conversion of powdered graphite into oxidize product. Additionally, the inter-planer distance of synthesized GO–ZrO<sub>2</sub> NC was found to be 2.94 Å and 1.77 Å.

FTIR analysis was done for a detailed investigation of metal–oxygen and carbon–oxygen bonding present in the synthesized GO, ZrO<sub>2</sub> and GO–ZrO<sub>2</sub> NC as shown in Fig. 2. The broad peak was observed at 3409 cm<sup>-1</sup> in case of GO, GO–ZrO<sub>2</sub> NC and ZrO<sub>2</sub> spectra, which is attributed to the presence of hydroxyl stretching bond. The infrared spectra of ZrO<sub>2</sub> nanoparticles show the sharp and intense stretching vibration bond at 772 cm<sup>-1</sup> and 663.20 cm<sup>-1</sup>. The obtained result corresponds to the presence of Zr–O metal–oxygen bonding associated with synthesized ZrO<sub>2</sub> nanoparticles. In the case of GO–ZrO<sub>2</sub> NC, due to the formation

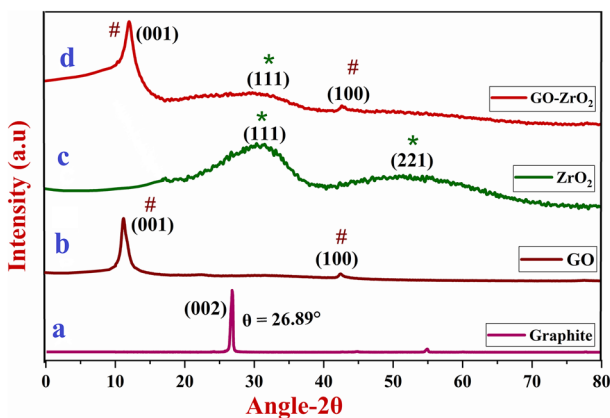
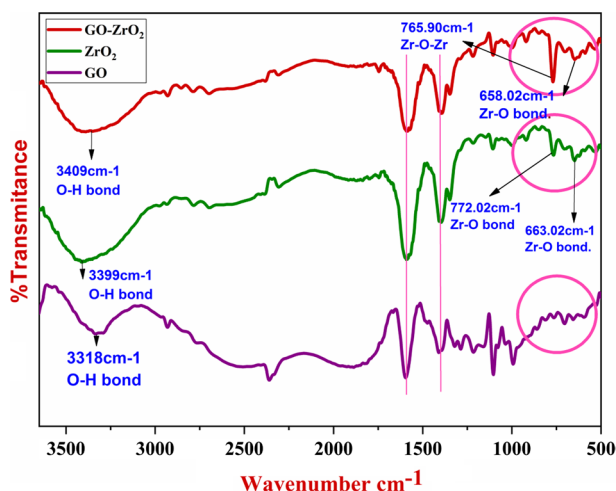


Fig. 1 X-ray diffraction patterns of given samples graphite, GO, ZrO<sub>2</sub> and GO–ZrO<sub>2</sub> NCs



**Fig. 2** FTIR spectra of GO, ZrO<sub>2</sub> and GO-ZrO<sub>2</sub> NC nanoparticles

of a hetero-junction between ZrO<sub>2</sub> and GO, the stretching vibration bond of the Zr-O bond was slightly shifted toward the lower frequency region at 764 cm<sup>-1</sup> and 658 cm<sup>-1</sup>. However, in the case of FTIR spectra of GO, there was no sharp peak in fingerprinting region. These observations signify the existence of a strong bonding nature between ZrO<sub>2</sub> and GO [35].

The intact morphology of the synthesized materials was analyzed by using field emission scanning electron microscopy (FESEM). Figure 3a reveals the formation of a multi-layered silky gauze form of GO sheet, while Fig. 3b indicates the larger agglomerated spherical shape of ZrO<sub>2</sub> nanoparticles. Additionally, after the closer investigation of Fig. 3c, d the surface of the GO sheet was unevenly decorated with the spherical shape of ZrO<sub>2</sub> nanoparticles with an average particle size of < 100 nm in the case of the synthesized GO-ZrO<sub>2</sub> NC. In order to determine the elemental composition of synthesis GO-ZrO<sub>2</sub> NC, energy dispersive spectroscopy (EDS) and elemental mapping were carried out as illustrated in Fig. 4. The closer investigation of EDS data reveals that the C, O and Zr elemental were unevenly present in the synthesized GO-ZrO<sub>2</sub> NC, as shown in Fig. 4a. Additionally, this haphazard distribution of these elemental (C, O and Zr) was strongly supported from the elemental mapping (specified by different colors) of synthesized GO-ZrO<sub>2</sub> NC as portrayed in Fig. 4b.

Furthermore, the successful formation of GO-ZrO<sub>2</sub> NC was examined by using HR-TEM analysis. The microstructure of synthesized GO-ZrO<sub>2</sub> NC reveals the heavy agglomerated spherical ZrO<sub>2</sub> nanomaterials, which are randomly dispersed over the surface of GO sheets as shown in Fig. 5a, b. This agglomeration of ZrO<sub>2</sub> nanoparticles might be due to heterogeneous nucleation and strong interfacial interaction between ZrO<sub>2</sub> nanoparticles and GO. The Fig. 5c indicates the parallel growth direction of ZrO<sub>2</sub> nanoparticles towards lattice fringes, and the calculated lattice spacing value of the plan (111) is 0.29 nm. This measured d-spacing value

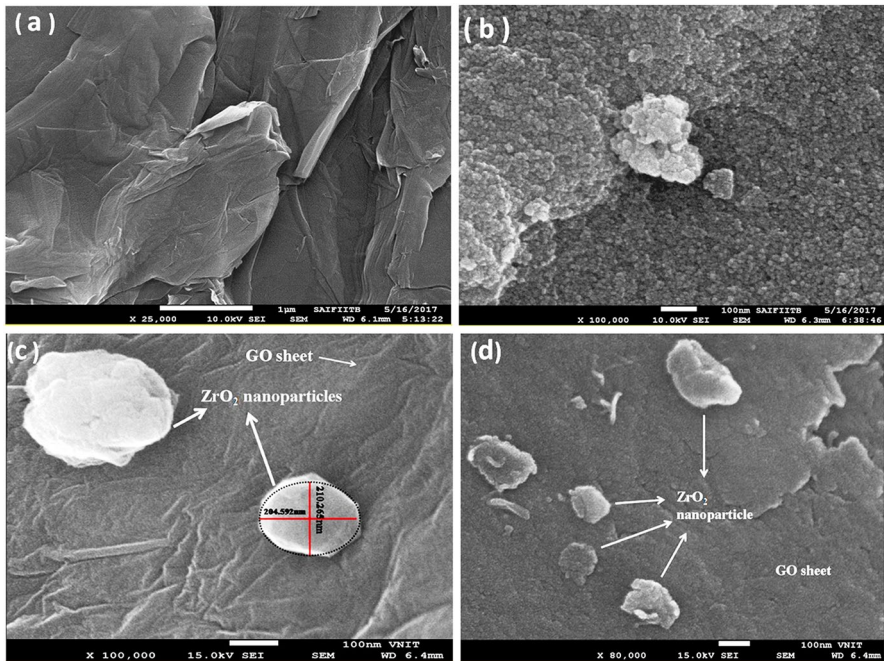


**Fig. 3** **a** FE-SEM image of GO sheets, **b**  $ZrO_2$  nanoparticles, **c**, **d** represent the FE-SEM image of synthesized GO- $ZrO_2$  NC

is very similar to that of d-spacing observed in XRD analysis of monoclinic  $ZrO_2$  nanoparticles. Additionally, the selected area electron diffraction (SAED) pattern of synthesized GO- $ZrO_2$  NC was shown in Fig. 5d, these diffraction rings were exactly matching to the planes observed in the XRD analysis.

The thermal stability of synthesized GO- $ZrO_2$  NC was studied by using TGA analysis as shown in Fig. 6. The pure  $ZrO_2$  nanoparticles, about 15% mass was a loss up to 200 °C, which might be due to the presence of moisture and further very minor mass loss may be leads to removal of interstitial hydroxyl groups and structural rearrangement during heating. In the case of synthesized GO- $ZrO_2$  NC shows about 20–25% mass loss at 100–200 °C, which might be due to the loss of water and solvents respectively. Moreover, the synthesized GO- $ZrO_2$  NC exhibited only 40% mass loss up to 900 °C while GO exhibits 55% mass loss up to 900 °C, which shows the enhanced thermal stability of synthesized GO- $ZrO_2$  NC as compared to bare GO.

The surface textural properties of synthesized GO- $ZrO_2$  NC was analyzed by  $N_2$  adsorption–desorption experiments at  $-196$  °C, and the further interpretation was made by using Brunauer–Emmett–Teller (BET) method. Figure 7 shows the  $N_2$  adsorption isotherm and pore size distribution curve of synthesized GO- $ZrO_2$  NC. The isotherms exhibit the features intermediate between the type-I and type-II isotherms as per IUPAC classification. The significant increase in the adsorption at low  $P/P_0$  and broad knee followed by long plateau and extent to small tail



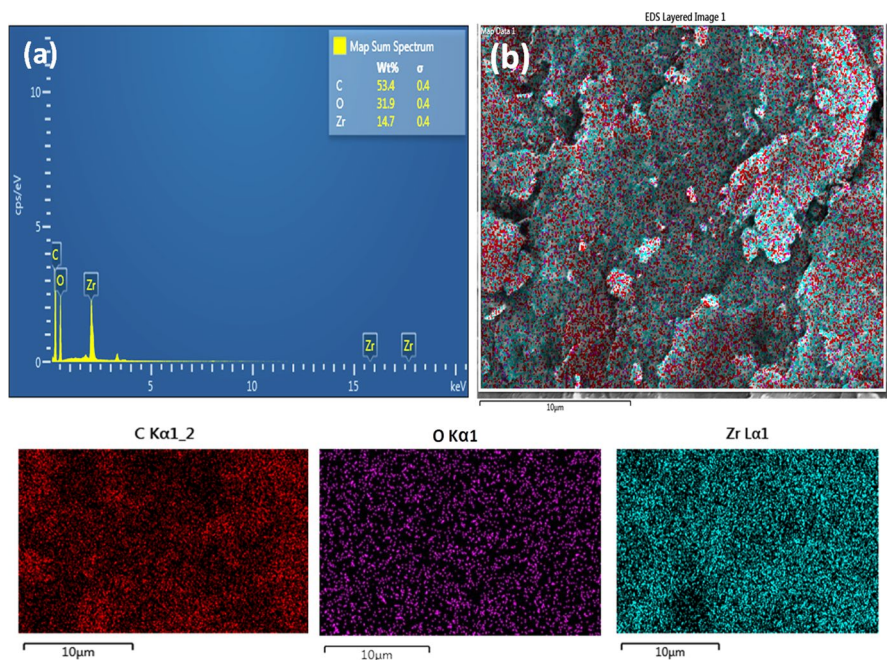


**Fig. 4** EDS and elemental mapping analysis of GO-ZrO<sub>2</sub> NC

with increases in relative pressure. Indicating the formation of porous network followed by mesoporous and small external surface area. The specific surface area of GO-ZrO<sub>2</sub> NC is 46.27 m<sup>2</sup>/g with an average pore size diameter of 3.19 nm, which significantly reveals the mesoporous nature. While the surface area of ZrO<sub>2</sub> nanoparticles and GO is found to be 245.14 m<sup>2</sup>/g and 19.58 m<sup>2</sup>/g with an average pore size of 2.55 nm and 5.30 nm, respectively, as given in Table 1. The lower surface area of GO-ZrO<sub>2</sub> NC compared to the ZrO<sub>2</sub> may be due to blocking of a few sites by GO in the ZrO<sub>2</sub> structure.

The UV-DRS analysis was carried out to calculate the optical band gap of synthesized GO-ZrO<sub>2</sub> NC and ZrO<sub>2</sub> as shown in Fig. 8. The optical band gap of synthesized bare ZrO<sub>2</sub> was found to be 3.5 eV, which restricts the photocatalytic efficiency of bare ZrO<sub>2</sub> nanomaterials in visible light irradiation. However, the optical band of synthesized GO-ZrO<sub>2</sub> NC was found to be 2.5 eV, which helps to harvest the visible light and overcome the all perpetual drawbacks like narrow spectral photoresponse and lower photocatalytic efficiency occurred due to the recombination. Thus, from this, the synthesized GO-ZrO<sub>2</sub> NC shows higher photocatalytic efficiency under visible light irradiation.

The recombination rate of the photogenerated electron-hole pair in the semiconductor materials was investigated via photoluminescence (PL) spectroscopic analysis as shown in Fig. 9. The PL emission spectra of GO-ZrO<sub>2</sub> NC and ZrO<sub>2</sub> were recorded in excitation wavelength of 359 nm at room temperature and the emission spectra emerged at 416 nm and 418 nm, showing a small blue shift, which shows a



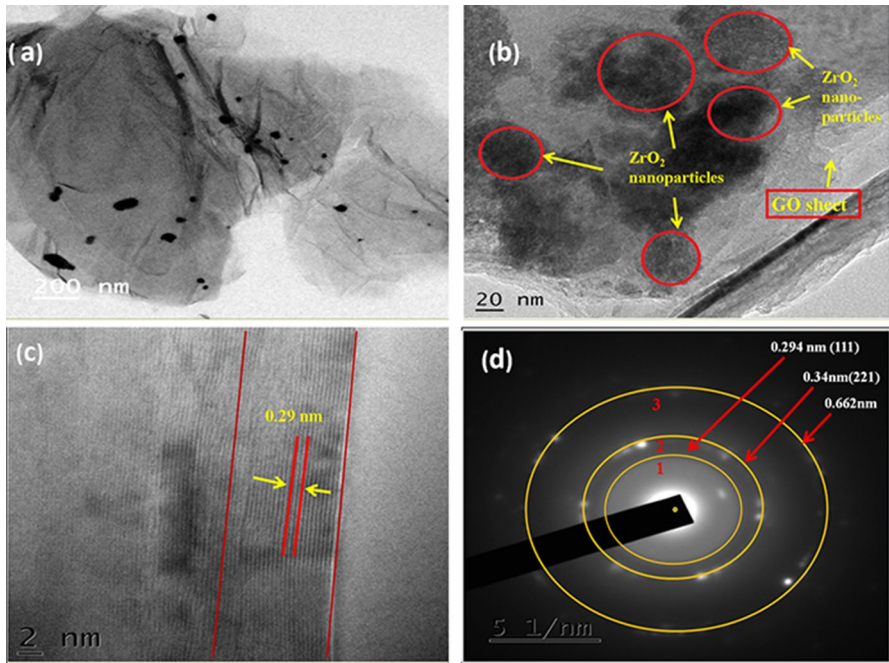


Fig. 5 a, b shows the HR-TEM image of GO-ZrO<sub>2</sub> NC, c HR-TEM image GO-ZrO<sub>2</sub> NC showing d-spacing value and, d shows the SEAD pattern of GO-ZrO<sub>2</sub> NC

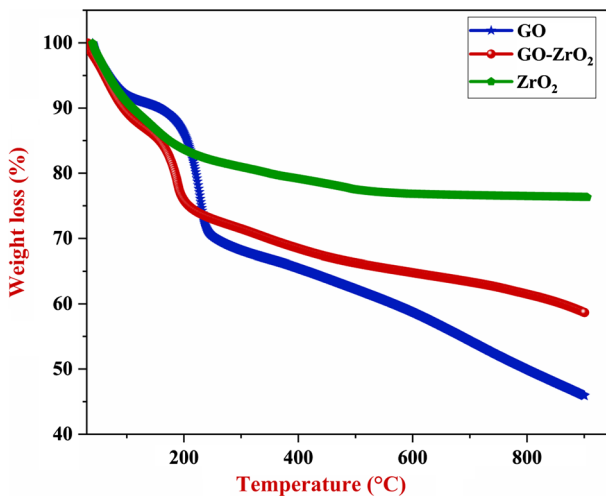


Fig. 6 TGA analysis of GO, ZrO<sub>2</sub> and GO-ZrO<sub>2</sub> NC

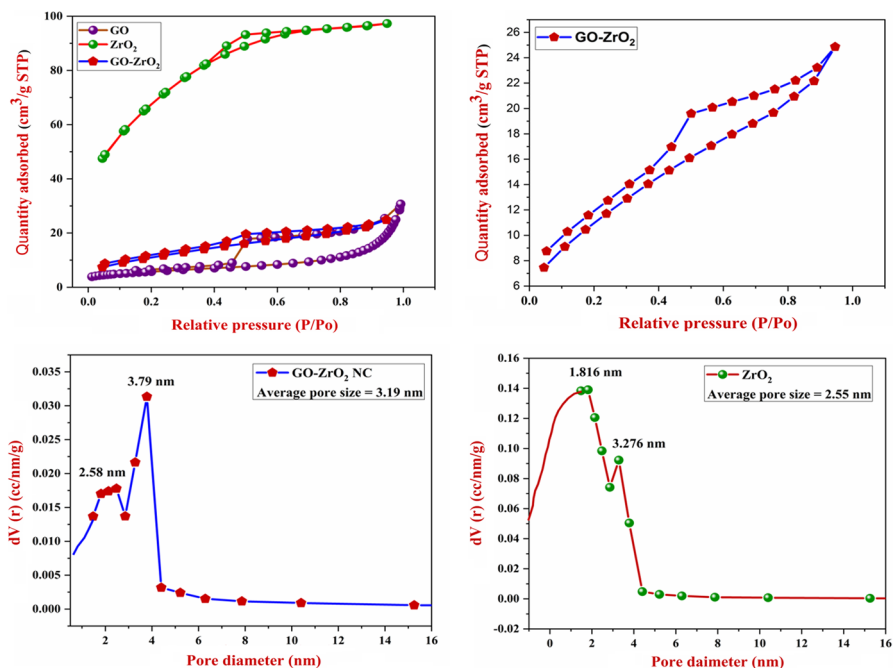


Fig. 7  $N_2$  adsorption isotherms of GO,  $ZrO_2$  and GO- $ZrO_2$  NC along with pore size distribution curve

Table 1 BET analysis of GO,  $ZrO_2$  and GO- $ZrO_2$  NC

Sr. no.	Samples	Surface area ( $m^2/g$ )	Pore volume ( $cc/g$ )	Pore size (nm)
1.	$ZrO_2$	245.14	0.14	1.81
2.	GO	19.58	0.99	5.30
3.	GO- $ZrO_2$	46.27	0.038	3.79

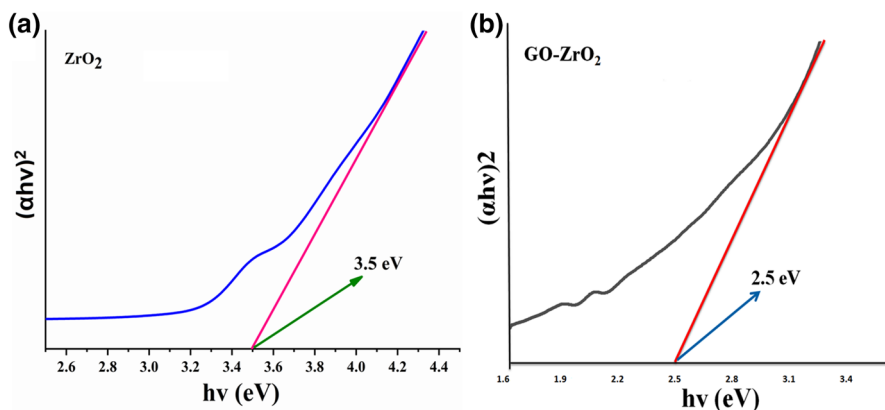
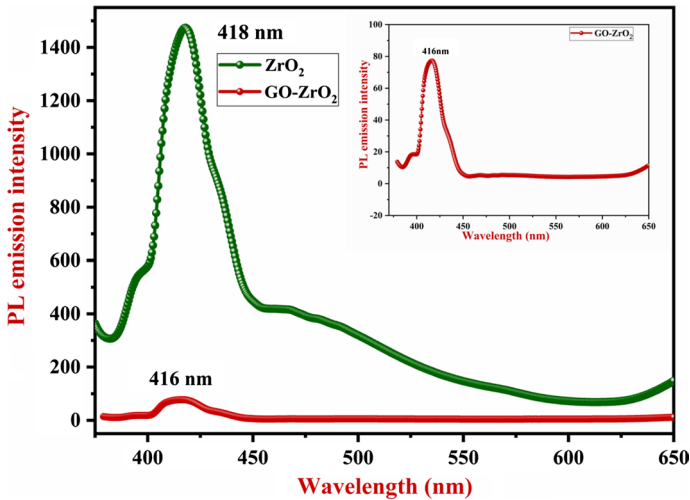


Fig. 8 UV-DRS spectra of  $ZrO_2$  and GO- $ZrO_2$  NC



**Fig. 9** Photoluminescence spectra of  $\text{ZrO}_2$  and  $\text{GO-ZrO}_2$  NC

good interaction between the metal oxide and GO. A nearly 18 times decrease in the intensity of emission spectra of  $\text{GO-ZrO}_2$  NC as compared to the bare  $\text{ZrO}_2$  nanoparticles shows the interface between  $\text{ZrO}_2$  and GO. These results illustrated the existence of efficient separation of photogenerated charge carrier due to the decreasing intensity of synthesized  $\text{GO-ZrO}_2$  NC in PL spectra, which suppressed the recombination rate of  $e^-/h^+$  pairs and enhance the photocatalytic degradation rate of organic pollutants. The mechanism involved is when  $\text{ZrO}_2$  nanoparticles are decorated on the surface of GO, the photogenerated electrons on the conduction band (CB) of  $\text{ZrO}_2$  transfer to the GO sheet. The presence of a conjugated  $\pi$ -system in GO delocalized the electrons on the surface of the GO sheet. This results in enhanced separation of  $e^-/h^+$  pairs, which leads to an increase the photocatalytic efficiency in the case of synthesized  $\text{GO-ZrO}_2$  NC as compared to their bare counterparts ( $\text{ZrO}_2$  and GO). Additionally,  $\text{Zr}^{+4}$  also shows strong bonding interaction with GO moiety rather than rGO due to the presence of a large number of oxygen-containing the functional group. This is supported by the improved photocatalytic activity of the synthesized  $\text{GO-ZrO}_2$  NC compared to reported rGO- $\text{ZrO}_2$  NC under the same reaction condition and is mentioned in supplementary file (Fig. S1) [9].

## Photocatalytic activity

The photocatalytic efficiency of synthesized  $\text{GO-ZrO}_2$  NC and  $\text{ZrO}_2$  was evaluated by using Rh-B and MB dye solutions as a model organic pollutant. Figure 10 shows the comparative photodegradation of Rh-B and MB dye solution under visible light irradiation. The change in the concentration of Rh-B dye solution with visible light irradiating time was monitored using UV-visible spectra (Fig. S2). In order to check the photocatalytic efficiency of synthesized  $\text{GO-ZrO}_2$  NC, several controlled

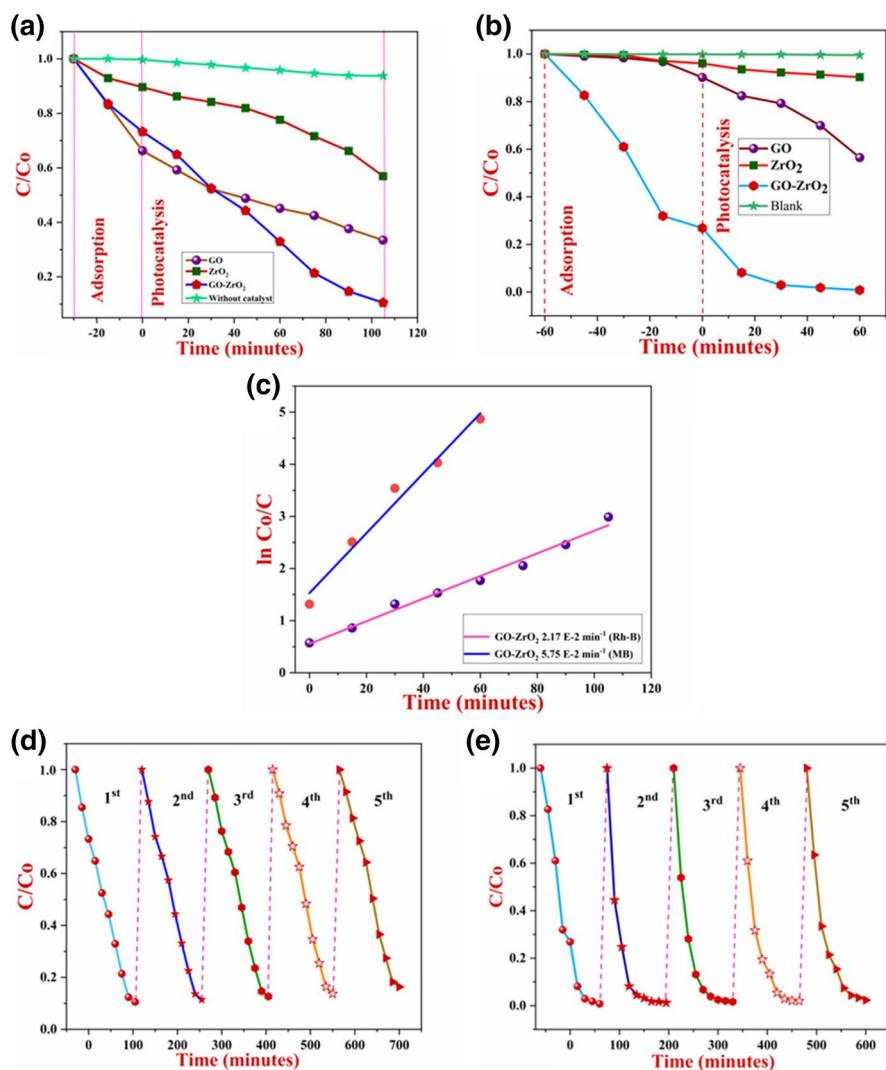


**Fig. 10** **a** Comparative analysis of photocatalytic degradation of Rh-B (30 mg/L concentration), **b** shows the comparative study of adsorptive photocatalytic degradation of MB dye solution (100 mg/L concentration), **c** kinetic study of both dyes, Rh-B and MB, **d**, **e** reusability of the catalyst

experiments were also carried out by using ZrO<sub>2</sub> and GO materials and without photocatalyst, as shown in Fig. 10a. In the absence of catalyst there is an insignificant decrease in the concentration of dye with time, which shows the lack of photosensitization and degradation in the absence of catalyst.

The photodegradation efficiency of Rh-B increases subsequently from ZrO<sub>2</sub> nanoparticles (40%), followed by the use of electron carrier GO (66.65%), and finally synthesized GO–ZrO<sub>2</sub> NC after irradiation for 105 min exhibits the

**Table 2** Photocatalytic degradation of 100 mL rhodamine B (Rh-B) dye solution (30 mg/L) using 25 mg GO-ZrO<sub>2</sub> NC

Sr. no.	Catalyst	Concentration (ppm)	Dose (mg)	Time (min)	% Adsorption	% Degradation
1.	ZrO <sub>2</sub>	30	25	105	7.11	40.02
2.	GO	30	25	105	16.87	66.54
3.	GO-ZrO <sub>2</sub>	30	25	105	45.62	90

**Table 3** Comparative study of photocatalytic degradation by using optimized concentration of methylene blue dye solution (100 mg/L)

Sr. no.	Catalyst	Concentration (ppm)	Dose (mg)	Time (min)	% Adsorption	% Degradation
1.	ZrO <sub>2</sub>	100	25	90	0.31	10.30
2.	GO	100	25	90	1.65	71.74
3.	GO-ZrO <sub>2</sub>	100	25	90	73.15	99.23

highest photodegradation efficiency of 90%. The enhanced photocatalytic activity of GO-ZrO<sub>2</sub> NC composite is due to the incorporation of ZrO<sub>2</sub> on GO, which magnifies the separation of e<sup>-</sup>/h<sup>+</sup> pairs. The comparative degradation efficiency of synthesized GO-ZrO<sub>2</sub> NC and bare counter parts (ZrO<sub>2</sub> and GO) are given in Table 2. Kinetics of Rh-B degradation was evaluated under similar reaction conditions as demonstrated in Fig. 10c. The synthesized GO-ZrO<sub>2</sub> NC follows the pseudo-first-order reaction kinetic with the rate constant  $K=2.1E-2 \text{ min}^{-1}$ , calculated by using the given Eq. (2).

$$-\ln \frac{C}{C_0} = kt \quad (2)$$

Similarly, the photodegradation of MB dye solution was examined by using the similar reaction conditions. The concentration of MB dye solution was optimized at a constant dose of the catalyst as given in Table S1 (supplementary information). The optimized concentration was selected for further photodegradation studies and results are portrayed in Fig. 10b. The adsorption and photodegradation results reveals that synthesized GO-ZrO<sub>2</sub> NC adsorbs 73.15% of dye solution and achieved the maximum adsorption-desorption equilibrium in 60 min, which on further irradiation with visible light for another 60 min results in 99.23% photodegradation of MB dye solution. The comparative photocatalytic study of synthesized GO-ZrO<sub>2</sub> NC and counterparts (ZrO<sub>2</sub> and GO) by using MB dye solution under ambient reaction condition was given in Table 3. From the comparative study, results revealed that GO-ZrO<sub>2</sub> NC degrades 99.23% MB dye solution in just 60 min of the time interval, which is higher than bare ZrO<sub>2</sub> (10.30%) and GO (71.45%). The photocatalytic degradation of MB dye follows the pseudo-first-order kinetic model with  $5.75E-2 \text{ min}^{-1}$  rate constant, which is considerably much higher as compared to the rate constant ( $2.1E-2 \text{ min}^{-1}$ ) of Rh-B degradation by using the same catalyst

(GO–ZrO<sub>2</sub> NC) as shown in Fig. 10c, which can be attributed to higher adsorption of MB on the GO–ZrO<sub>2</sub> NC. Hence, the synthesized GO–ZrO<sub>2</sub> NC provides a great probability to acts as a superior material showing both the property of adsorbent as well as photocatalyst for environmental remediation. For practical application of the catalyst, reusability and stability is a major concern, thus in order to check the stability and reusability of the catalyst, GO–ZrO<sub>2</sub> NC has been reused for five successive experimental cycles as displayed in Fig. 10c, d. The figure clearly reveals that the synthesized GO–ZrO<sub>2</sub> NC retained almost 95% degradation even after five consecutive cycles and illustrates the excellent reproducibility and high stability. To establish the superiority of our synthesized GO–ZrO<sub>2</sub> NC, we have compared the adsorption and photocatalytic degradation efficiency of synthesized GO–ZrO<sub>2</sub> NC with other already reported similar materials given in Table 4. From Table 4, it can be concluded that this synthesized GO–ZrO<sub>2</sub> NC has much higher adsorption, as well as photocatalytic efficiency than the previously reported doped and undoped GO–ZrO<sub>2</sub> materials.

To understand the detailed mechanism and reactive oxygen species (ROS) participated in the photodegradation of dye solution, the trapping experiment was carried out over GO–ZrO<sub>2</sub> nanocomposite under visible light irradiation by using radical scavengers. In this experiment 1 mmol of Benzoquinone (BQ), Isopropyl alcohol (IPA), Ammonium oxalate (AO) and Silver nitrate (SN) were added in order to trapped superoxide (O<sub>2</sub><sup>-</sup>), hydroxyl radicals (OH<sup>·</sup>), holes (h<sup>+</sup>) and electron (e<sup>-</sup>) radicals, respectively. Results reveal that the photodegradation of Rh-B was considerably suppressed by using BQ (60%), about 16% by IPA, 8% by AO and only 6% of dye degradation was suppressed by SN, as shown in Fig. 11a. Thus, here we conclude that the superoxide radical (O<sub>2</sub><sup>-</sup>) is the most primary active species in the photodegradation of Rh-B dye solution.

The plausible photodegradation mechanism by using synthesized GO–ZrO<sub>2</sub> NC is shown in Fig. 11b. In detailed, the ZrO<sub>2</sub> nanoparticles decorated on the surface of GO sheet of the composite, possibly excited and induced photogenerated e<sup>-</sup>/h<sup>+</sup> pairs under the visible light irradiation as shown in Eq. (3). The photogenerated electron gets migrate from the conduction band (CB) of ZrO<sub>2</sub> nanoparticles to the surface of GO (Eq. 4) and reduced oxygen molecule results in the formation of superoxide radicals O<sub>2</sub><sup>-</sup> (Eq. 5). In addition, the electron deficiency (hole) on valence band (VB) is responsible for the formation of hydroxyl radical (OH<sup>·</sup>) as given in Eq. (6). The key reactive species constitute during the photodegradation studies namely superoxide radicals (O<sub>2</sub><sup>-</sup>) and hydroxyl radicals (OH<sup>·</sup>) are mainly responsible for the degradation of organic pollutants into eco-friendly degradation product i.e. CO<sub>2</sub> and H<sub>2</sub>O molecules (Eq. 8).

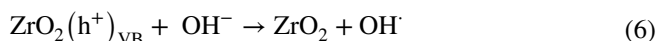
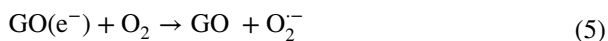
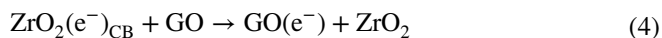
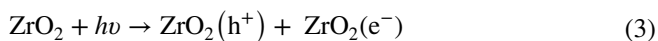




**Table 4** Comparative study of photocatalytic degradation by using catalyst GO-ZrO<sub>2</sub> with different concentrations, doses, time and model organic pollutant

Sr. no.	Name of adsorbent/ photocatalyst	Method of preparation	Particle Size	Surface area (m <sup>2</sup> / gm)	Adsorbate/ pollutant	(Concentration)	Dose ADSORBENT/photocatalyst (mg)	Time (min)	%Efficiency	Rate constant	References
1.	GO-ZrO <sub>2</sub> (adsorption)	Post-grafting Method	*	160.1	Phosphate ion	10 ppm	200	550	90% (Adsorption)	$2.52E-3 \text{ min}^{-1}$	[17]
2.	Graphene/ZrO <sub>2</sub>	Sol-gel Method	*	89	P-Nitrophenol	10 ppm	50	90	*	*	[29]
3.	Nd-doped ZrO <sub>2</sub> -GO	Co-precipitation Method	*	*	Eosin Y dye	20 ppm	100	180	*	$4.19E-3 \text{ min}^{-1}$	[31]
4.	GO-ZrO <sub>2</sub>	Co-precipitation Method	< 100 nm	46.27	Rhodamine-B (Rh-B) and methylene blue (MB)	30 ppm	25	105 for Rh-B 60 for MB	90% for Rh-B and 99.23% for MB	$2.1E-2 \text{ min}^{-1}$ $5.75E-2 \text{ min}^{-1}$	Present work

\*Means % efficiency is not mention

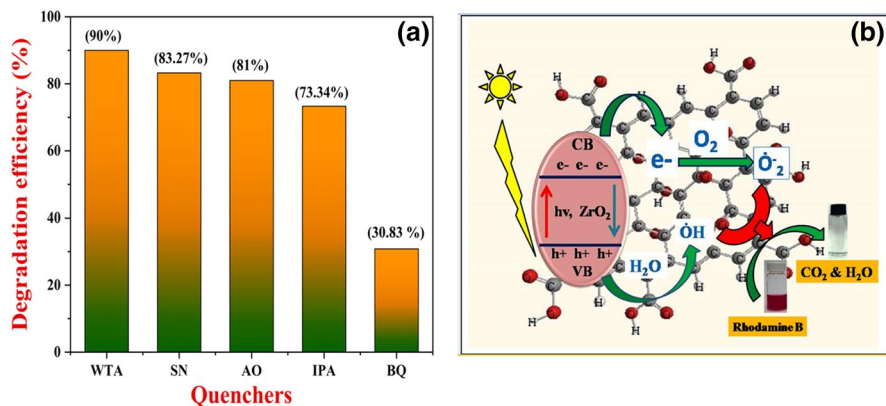
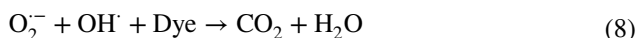
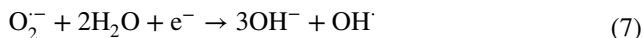


Fig. 11 Illustration the trapping experiment along with photocatalytic mechanism of GO–ZrO<sub>2</sub> NC



From this discussion, this current room temperature mediates synthesis method is the most superior method for the synthesized GO–ZrO<sub>2</sub> NC.

## Conclusion

In conclusion, we synthesized GO–ZrO<sub>2</sub> NC through a facile co-precipitation method at room temperature. The formation of GO–ZrO<sub>2</sub> NC was confirmed by using several characterization techniques. The characterization results showed that the synthesized GO–ZrO<sub>2</sub> NC were amorphous in nature and exhibit a monoclinic phase of ZrO<sub>2</sub> in composite with spherical morphology displaying narrow band gap compared to bare ZrO<sub>2</sub> nanoparticles. The decreasing PL emission intensity of GO–ZrO<sub>2</sub> NC suggested the good interaction between ZrO<sub>2</sub> and GO, which improved the electron–hole separation, leading to enhanced photocatalytic efficiency. The photocatalytic experimental results revealed that GO–ZrO<sub>2</sub> NC degrades Rh-B, MB and RB4 dyes in the same reaction condition by 90%, 99.23% and 83.58%, respectively. Based on our investigations and obtained experimental results we concluded that synthesized GO–ZrO<sub>2</sub> NC is an excellent photocatalyst, as well as very good adsorbent and also possesses excellent reproducibility and stability up to five successive cycles.

**Acknowledgements** We would like to thank the director, VNIT, Nagpur, India, for providing financial assistance. We are also thankful to the Sophisticated Test and Instrumentation Center, Kerala, Cochin University, for providing instrument facility for our research work. We are also thankful to Punjab University, Chandigarh, and SAIF Madras, for providing the instrumental facility. We are also thankful to the Dr. R. S. Gedam, Department of Physics, VNIT, Nagpur,, for providing the instrumental facility.

## References

1. A. Quintana, A. Altube, E. Garcia-Lecina, S. Surinach, M.D. Baro, J. Sort, E. Pellicer, M. Guerrero, *J. Mater. Sci.* **52**, 13779 (2017)
2. S.K. Warkhade, G.S. Gaikwad, S.P. Zodape, U. Pratap, A.V. Maldhure, A.V. Wankhade, *Mater. Sci. Semicond. Process.* **63**, 18 (2017)
3. E.S. Agorku, A.C. Pandey, B.B. Mamba, A.K. Mishra, *Mater. Today Proc.* **2**, 3909 (2015)
4. S. Allahveran, A. Mehrizad, *J. Mol. Liq.* **225**, 339 (2016)
5. E.B. Yazdani, A. Mehrizad, *J. Mol. Liq.* **255**, 102 (2018)
6. S. Rani, M. Aggarwal, M. Kumar, S. Sharma, D. Kumar, *Water Sci.* **30**, 51 (2016)
7. D. Liu, S. Deng, A. Maimaiti, B. Wang, J. Huang, Y. Wang, G. Yu, *J. Colloid Interface Sci.* **511**, 277 (2018)
8. E.S. Agorku, A.T. Kuvarega, B.B. Mamba, A.C. Pandey, A.K. Mishra, *J. Rare Earths* **33**, 498 (2015)
9. S.O.B. Oppong, W.W. Anku, S.K. Shukla, P.P. Govender, *Res. Chem. Intermed.* **43**, 481 (2017)
10. P. Bakhtkosh, A. Mehrizad, *J. Mol. Liq.* **240**, 65 (2017)
11. A. Mehrizad, P. Gharbani, *Photochem. Photobiol.* **93**(5), 1178 (2017)
12. F. Ciesielczyk, W. Szczekocka, K. Siwińska-stefańska, A. Piasecki, *Open Chem.* **15**, 7 (2017)
13. N. Prabhakarao, M.R. Chandra, T.S. Rao, *J. Alloys Compd.* **694**, 596 (2017)
14. A. Mehrizad, P. Gharbani, *J. Water Health* **15**(6), 955 (2017)
15. K. Gurushantha, K.S. Anantharaju, L. Renuka, S.C. Sharma, *RSC Adv.* **7**, 12690 (2017)
16. R. Ali, K. Rao, S. Singh, B. Raj, W. Khan, A.H. Naqvi, *J. Environ. Chem. Eng.* **2**, 199 (2014)
17. E. Zong, D. Wei, H. Wan, S. Zheng, Z. Xu, D. Zhu, *Chem. Eng. J.* **221**, 193 (2013)
18. J. Zhang, N. Chen, M. Li, P. Su, C. Feng, *React. Funct. Polym.* **114**, 127 (2017)
19. H. Teymourian, A. Salimi, S. Firoozi, *Electrochim. Acta* **143**, 196 (2014)
20. B.R. Singh, M. Shoeb, W. Khan, A.H. Naqvi, *J. Alloys Compd.* **651**, 598 (2015)
21. X. Wang, L. Zhang, H. Lin, Q. Nong, Y. Wu, *RSC Adv.* **4**, 40029 (2014)
22. Y. Ke, H. Guo, D. Wang, J. Chen, W. Weng, *J. Mater. Res.* **29**, 2473 (2014)
23. F. Lupo, R. Kamalakaran, C. Scheu, N. Grobert, M. Ruhle, *Carbon* **42**, 1995 (2004)
24. R. Saada, S. Kellici, T. Heil, D. Morgan, B. Saha, *Appl. Catal. B Environ.* **168–169**, 353 (2015)
25. A. Mehrizad, P. Gharbani, *Pol. J. Environ. Stud.* **23**, 2111 (2014)
26. P.P.A. Jose, M.S. Kala, N. Kalarikkal, S. Thomas, *Res. Chem. Intermed.* **44**(9), 5597 (2018)
27. F. Davar, A. Majedi, A. Abbasi, *J. Mater. Sci.: Mater. Electron.* **28**, 4871 (2017)
28. S.M. El-Dafrawy, M. Farag, S.M. Hassan, *Res. Chem. Intermed.* **43**, 6343 (2017)
29. S.N. Basahel, M. Mokhtar, E.H. Alsharaeh, T.T. Ali, H.A. Mahmoud, K. Narasimharao, *Nanosci. Nanotechnol. Lett.* **8**, 448 (2016)
30. H. Mudila, S. Rana, M.G.H. Zaidi, *J. Anal. Sci. Technol.* **7**, 3 (2016)
31. M. Mzoughi, W.W. Anku, S.O.B. Oppong, S.K. Shukla, E.S. Agorku, P.P. Govender, *Adv. Mater. Lett.* **7**(11), 100 (2016)
32. X. Luo, C. Wang, L. Wang, F. Deng, S. Luo, X. Tu, C. Au, *Chem. Eng. J.* **220**, 98 (2013)
33. B. Prashanti, T. Damodharam, *J. Nanosci. Technol.* **3**, 256 (2017)
34. J. Chen, B. Yao, C. Li, G. Shi, *Carbon* **64**, 225 (2013)
35. X. Chen, Y. Liu, X. Xia, L. Wang, *Appl. Surf. Sci.* **407**, 470 (2017)